Chapter 1
Introduction & Literature Survey

1.1 General Introduction

Every human being needs energy, which is a very fundamental and necessary thing and it contributes significantly to the economic growth of any nation. World populations are rising exponentially and in proportion to that, the demand for energy is also increasing speedily. Seeing the energy consumption rate in the current scenario, it is predictable to increase by 65% by the year 2030, taking 2004 as the base year [1]. India ranks fourth in terms of energy consumption, behind the United States, China, and Russia [1]. Data analysis reveals that India's per capita total power consumption was 917.2 kWh as of March 2013 [2], and that by 2021-22, it is expected to reach approximately 2280 BkWh. In the upcoming years by 2031–32, it is expected that this figure will touch 4500 BkWh [3], indicating the huge shortage of electricity which works as a barrier to the development of the country. Therefore it is required to bring such processes which fulfil the demand of energy requirements of the growing world population and avoid the energy crisis. Presently, most of the energy used worldwide is obtained from thermal power plants which use fossil fuels (coal, oil, petroleum) as a non-renewable energy source and in India, a big portion of the energy is obtained from these power plants, almost 70% of the total installed capacity of the power plant [4]. Consumption of energy in such a way produces over-dependency on fossil fuels and raises a threat to the conservation of fossil fuels for our upcoming generation. These thermal power plants run on fossil fuels cause serious health problems and emit greenhouse gases such as carbon dioxide (CO_2), NO_x and SO_x. These greenhouses gases largely assist the global warming, affecting the climate and environment badly [5]. "Future of the sea: Biological responses to ocean warming'' reported that from 1870-1899 which is regarded as the pre-industrial times to the 2005-2014, a 0.7 ºC increment in the sea surface temperature was seen [6]. This flow of

temperature constantly rises, and seeing the emission levels of greenhouse gases, it is expected that by the end of 2100, a temperature hike between 1.2 ºC and 3.2 ºC will be noticed globally on the sea surface [6]. Seeing this scenario and encountering the ever-increasing energy requirements worldwide, Renewable energy sources (RES) provide clean and sustainable energy substitutes. Wind, Solar, hydroelectric, geothermal, and water-splitting (H_2 and O_2) are RES and by approaching these sources, we can reduce our dependency on fossil fuels. Many countries worldwide are taking steps and adopting the application of RES to become energy independent and reduce the energy crisis. On May 4, 2022, a meeting is held in Paris, where French President Emmanuel Macron and Indian Prime minister Narendra Modi gave a clear endorsement to encourage the bilateral cooperation on Hydrogen. Among the RES, solar and wind energy show encouraging interest in their use worldwide, but their behaviour is transient and requires proper energy management and storage system which is a costly process to operate. Geothermal energy is location specific and sometimes becomes the reason for earthquakes. In the hydroelectric process, for energy generation, a huge amount of water has to be stored which is very tedious and threatful as it causes floods during monsoons. Hydrogen (H_2) is viewed as a greener and clean energy and it is produced through water splitting, an electrochemical process, which is regarded as a sustainable and renewable method. Currently, it is regarded as the eye-catching technology for the production of H_2 and O_2 to replace fossil fuel energy in energy conversion and storage systems [7].

1.2 Water-splitting

1.2.1 History of water-splitting

An electrochemical reaction called water-splitting uses electrical energy to fragment the water (H_2O) into hydrogen (H_2) and oxygen (O_2). Hydrogen evolution reaction (HER) and oxygen evolution reaction (OER) are two of its half process. While OER uses a four-

electrons and four protons linked process, HER uses two two-electron and two proton-coupled mechanisms. Even in our prehistoric era, references to the splitting of water into H_2 and O_2 are made. This process dates back more than 200 years [9].

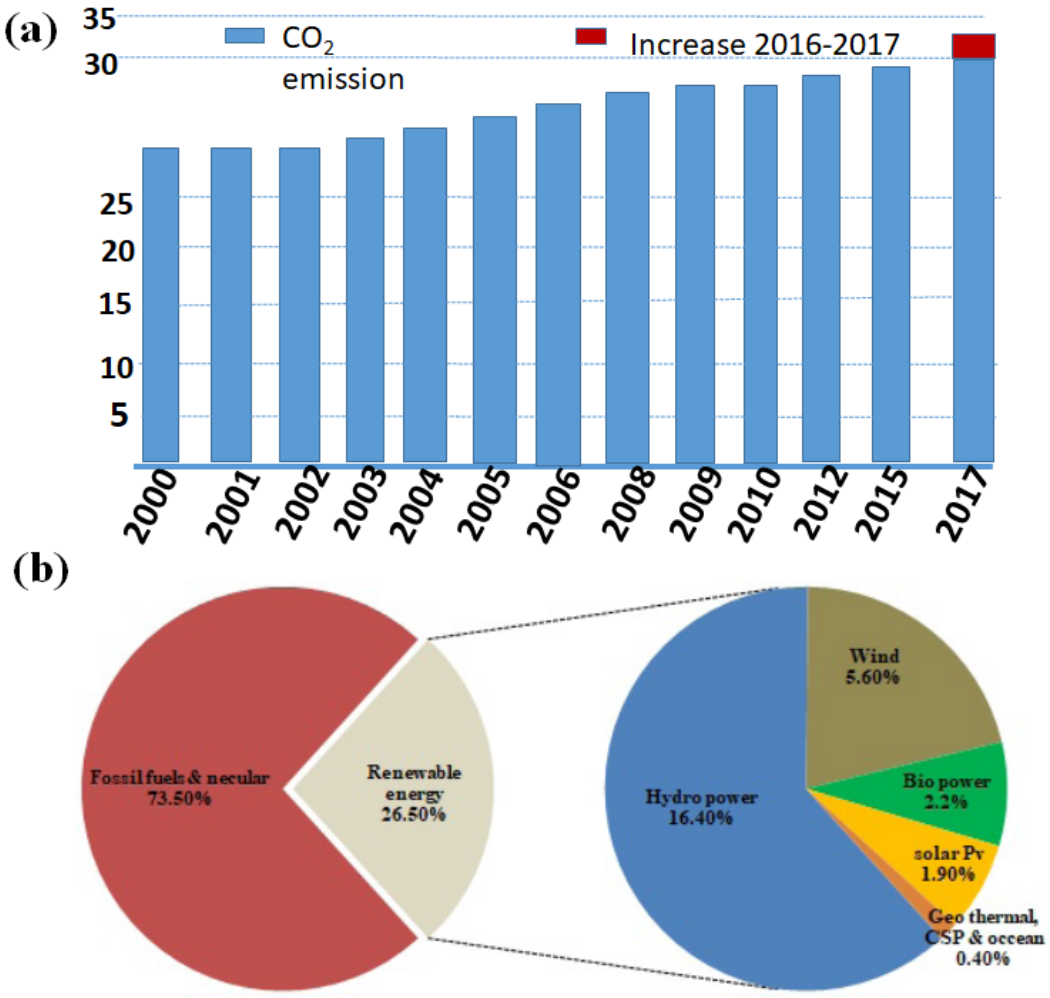

Figure 1.1 Overview of (a) Total CO_2 emission from the consumption of energy (fossil fuels) for the period of 2000-2017 and (b) contribution of RES in the production of electricity at a global level for the year 2017 [8].

Agastaya Samhita elucidates H_2 and O_2 by splitting water molecules using a dry cell with copper sulphate and zinc amalgamate, producing 23 mA current at 1.138 volts. The observations about this phenomenon were first recognised in 1789 and in 1800, Nicholson and Carlisle first developed this technique for industrial water electrolysis. For the experiment, they took a small tube, filled with water mounted vertically and sealed it. At

the one end of the tube, a platinum wire is inserted which is connected to the terminals of a voltaic pile. As the tips of the wire slowly approached each other, a spurt of bubbles was created from each of the tip. They called it oxygen and hydrogen, respectively. With a 10000 Nm^3 H_2/h capacity, a large-scale H_2 production operation was launched in 1939 using a water electrolysis facility. The thermodynamic potential to split water into hydrogen and oxygen is 1.23 V, but a cell voltage of 1.85-2.05 V is required to achieve 1A cm^{-2} current density, resulting in a conversion efficiency of just 60-66.5% with a loss of 33.5-40% in electricity [11].

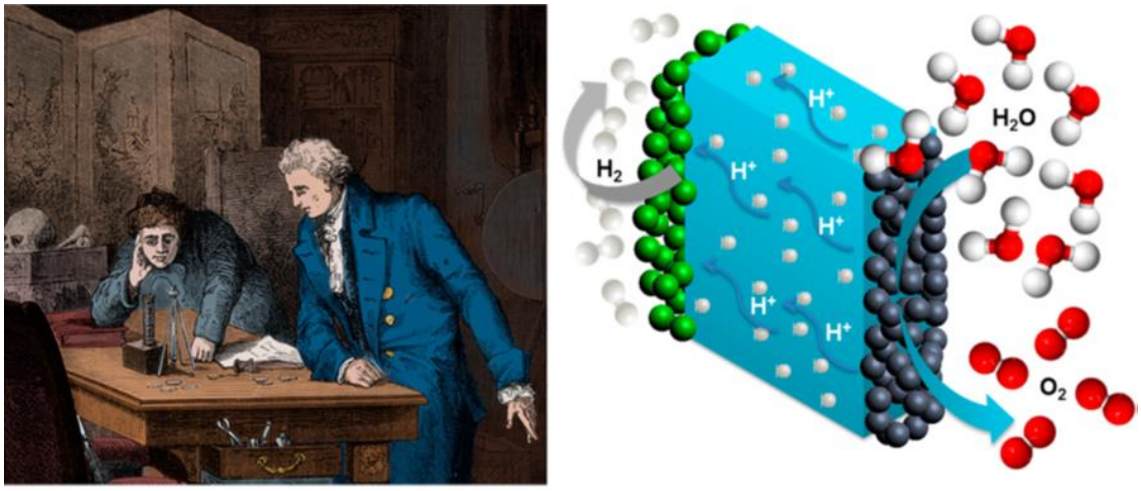

Figure 1.2 A picture depicting the water-splitting experiment by William Nicholson and Anthony Carlisle. On the left side, an observation of electrolysis by William Nicholson and Anthony Carlisle and on the right side, a schematic of the electrolyzer showing water oxidation on the anodic electrode (grey spheres) and hydrogen evolution on the cathodic electrode (green spheres) [10].

Electrochemical water-splitting technology has the potential to produce green hydrogen gas [12]. With no emissions of pollution, this hydrogen gas serves as an ultra-high energy carrier for a variety of applications. But, the sluggish kinetics and high overpotential of OER highly affect the efficiency of water electrolysis. Metal-air batteries, splitting of water, and fuel cells are the simplest, most effective, and inexhaustible approaches to producing as well as storing energy through electrochemical reactions. The fundamental

reactions that result in the reversible process in each of these systems are WOR (water oxidation reaction), also termed as OER, HER and ORR [13].

1.2.2 Water- splitting at different pH and thermodynamic feasibility

1.2.2.1 Water-splitting at pH=7 (pure water)

Due to insufficient self-ionization, pure water is a poor conductor of electricity **(**conductance one millionth than that of seawater). As a result, electrolysis of pure water is a very time-consuming process, and extra energy is needed in the form of over-potential to get past the various activation barriers. Without this extra energy, the process proceeds sporadically or even never.

At pH =7 and 25℃, electrolysis of pure water takes place as shown below (Eq. 1.1-1.3):

Half reaction at the cathode: $2H_2O\ (l) + 2e^- \rightarrow\ H_2\ (g) + 2OH^-\quad E^0 = -0.42\ V$

Half reaction at the anode: $2H_2O\ (l)\ \rightarrow\ O_2(g) + 4H^+ + 4e^-\quad E^0 = +0.82\ V$

Overall reaction: $2H_2O\ (l)\ \rightarrow\ \ 2H_2\ (g) + O_2\ (g)\quad E^0 = -1.24\ V$

Since the overall reaction has a negative cell potential and is therefore thermodynamically unfavourable, it can only occur at an external voltage of 2.4 V. A further, voltage (over potential) of around 0.6 V is needed at each electrode to keep the reaction going because of the low ion concentration and interfaces where electrons must pass. Electrolysis can be made more effective by using electrocatalysts and a suitable electrolyte such as salt, acid or base.

1.2.2.2 Water-splitting in the presence of acid (pH lower than 7)

In the presence of an acid, more hydrogen ions (H^+) are created, which are reduced at the negative electrode while water is oxidized at the positive electrode. The reaction takes as follows in the presence of acid at 25℃ (Eq. 1.4-1.6):

Half reaction at cathode: $2H^+ + e^- \rightarrow H_2(g)$ $E^0 = +0.0\,V$

Half reaction at anode: $2H_2O\,(l) \rightarrow O_2(g) + 4H^+ + 4e^-$ $E^0 = +1.23V$

Overall reaction: $2H_2O\,(l) \rightarrow O_2\,(g) + 2H_2\,(g)$ $E^0 = -1.23\,V$

Since the electrode potential (E^o) for overall reaction is negative, it is a thermodynamically unfeasible process but in comparison to pure water, the reaction occurs at a much lower potential.

1.2.2.3 Water-splitting in the presence of a base (pH higher than 7)

In the presence of a base, additional hydroxyl ions (OH^-) are produced which oxidise at the anode into O_2 by releasing their electrons while water molecules at the cathode are reduced into H_2. The reaction takes as follows in the presence of base at 25°C (Eq. 1.7-1.9):

Half reaction at cathode: $2H_2O\,(l) + 2e^- \rightarrow H_2\,(g) + 2OH^-$ $E^0 = -0.83\,V$

Half reaction at anode: $4OH^- \rightarrow O_2 + 2H_2O + 4e^-$ $E^0 = +0.4\,V$

Overall reaction: $2H_2O\,(l) \rightarrow O_2\,(g) + 2H_2$ $E^0 = -1.23\,V$

The electrode potential for the overall reaction is the same as in the acid medium.

1.3 Oxygen evolution reaction (OER)

Technologies for energy conversion and storage (ECS) such as fuel cells, water electrolyzers, and metal-air batteries are essential for the global transition away from fossil fuels. With the aid of these technologies, we are able to generate and store renewable energy in chemical forms while also further transforming it into electricity when it is needed [14, 15]. OER, which is regarded as a reliable mechanism for producing pure oxygen quickly, is essential for these ECS devices because it serves as a carrier by providing electrons in the electrochemical cycles that convert chemical fuels into power [13]. In a water electrolyzer, chemical fuels are generated through the water-splitting

followed by the OER at the anode [16]. While in metal-air batteries (MAB), OER occurs on the cathode and the performance of MAB during charging and discharging is directly influenced by the activity and stability of OER [17, 18]. In fuel cells, only when OER is present, is long-term energy storage and its eventual transformation into electrical energy again feasible [19]. Therefore, by converting and storing renewable energy, a close-cycle clean energy structure can be projected by increasing OER efficiency.

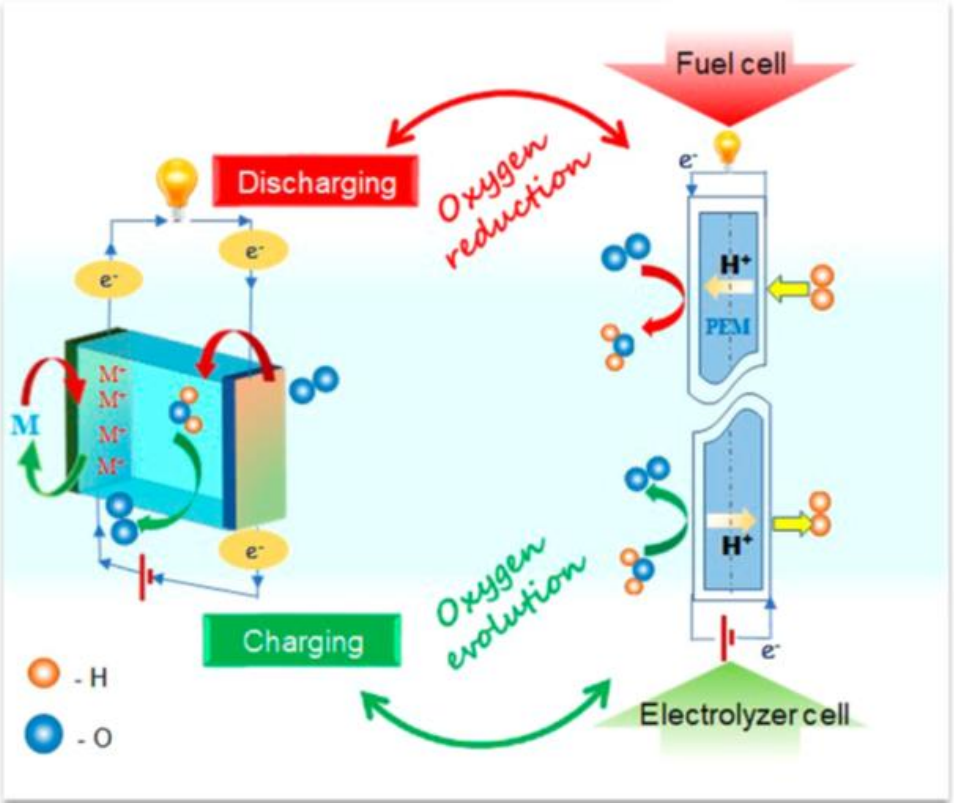

Figure 1.3 Figure showing the cyclic form of OER and ORR processes in electrolyzer cell, metal-air batteries and fuel cells [20].

1.3.1 OER in water splitting

In water splitting, OER or water oxidation reaction is the main obstruction that hinders energy conversion effectiveness due to its slow kinetics [20]. It occurs at the anode and O=O (O_2) bond formation takes place through the four consecutive proton-coupled electron transfer steps [21-23]. Due to multistep, several reaction intermediates are

generated which impose large reaction overpotential and sluggish kinetics. The OER reaction is highly pH dependent and the equilibrium half-cell potential (E_a^0) for this at 1 atm and 298 *K* (25 °C) in terms of standard hydrogen electrode (SHE) or normal hydrogen electrode (NHE) are defined as follows (Eq. 1.10-1.12)-

$$At\ pH = 0;\quad 2H_2O \rightarrow\ O_2 + 4H^+ + 4e^-\quad E_a^0 = 1.23\ V$$

$$At\ pH = 7;\ 2H_2O \rightarrow\ O_2 + 4H^+ + 4e^-\quad E_a^0 = 0.817\ V$$

$$At\ pH = 14;\ 4OH^- \rightarrow\ O_2 + 2H_2O + 4e^-\quad E_a^0 = 0.404\ V$$

At pH=0, HER occur at 0.0 V, and OER occurs at a high potential of 1.23 V, so to create the potential difference of 1.23 V *versus* SHE an external current is essential to facilitate the OER. Accordingly to the Nernst equation, theoretically,~ 59 mV shift in reaction potential is observed per unit pH [24]. As a result, the working potential of 1.23 V is maintained by using a reversible hydrogen electrode (RHE) as a reference electrode to prevent pH effects on the applied voltage.

1.3.1.1 Mechanism of OER

In general, there are two ways to describe the OER mechanism: adsorbate evolution mechanism (AEM) and lattice-oxygen-mediated mechanism (LOM) [25, 26].

1.3.1.1 (a) Adsorbate evolution mechanism (AEM)

According to the AEM, OER contains four elementary steps in both acidic and alkaline conditions with four electron/ proton transfer steps. In an acidic medium, O_2 gas is produced with the oxidation of water molecules with the simultaneous generation of four protons (H^+) and four electrons (e^-) pairs. Whereas, in an alkaline medium, O_2 is produced from the oxidation of hydroxyl groups (OH^-) into H_2O accompanied by the transfer of four electrons.

1.3.1.1 (a) (i) In an Acidic medium

At p=1 bar and T= 298.15 K the overall water oxidation reaction [21, 23]

$2H_2O\ (l) \rightarrow\ O_2\ (g) +\ 4H^+ + 4e^-;\ \Delta G_0 = 4.92\ eV$ (Eq. 1.13)

Takes place in four steps [21, 23] (Eq. 1.14-1.17)-

$$Step\ 1: H_2O\ (l) +\ M\ \rightarrow\ M - OH + H^+ + e^-$$

$$Step\ 2:\ \ M - OH\ \rightarrow M - O + H^+ +\ e^-$$

$$Step\ 3: H_2O\ (l) + M - O\ \rightarrow M - OOH + H^+ +\ e^-$$

$$Step\ 4: M - OOH\ \rightarrow M +\ O_2 +\ H^+ + e^-$$

1.3.1.1 (a) (ii) In an alkaline medium

At p=1 bar and T= 298.15 K, the OER reaction [22]

$4\ OH^- \rightarrow\ O_2\ (g) + 2H_2O\ (l) + 4e^-$ (Eq. 1.18)

Takes place in four elementary steps as follows [22, 23, 27] (Eq. 1.19-1.22) -

$$Step\ 1: M +\ OH^- \rightarrow M - OH +\ e^-$$

$$Step\ 2: M - OH +\ OH^- \rightarrow M - O + H_2O\ (l) + e^-$$

$$Step\ 3: M - O +\ OH^- \rightarrow M - OOH + e^-$$

$$Step\ 4: M - OOH +\ OH^- \rightarrow M +\ O_2\ (g) + H_2O\ (l) + e^-$$

Where, M denotes the active site of the catalyst (*), M-OH, M-O and M-OOH shows the adsorbed species on the active site of the catalyst. 'g' and 'l' refers to the gas and liquid phase of the species.

The first electron transfer occurs when H_2O (in an acidic medium) and OH^- (in a basic medium) adsorb on the active site of the electrocatalyst, which is typically an oxygen-coordinated metal. This results in the formation of an adsorbed OH species (M-OH) (step 1). Then through a second electron transfer this M-OH is oxidised to M-O (step 2). The M-OOH intermediate is generated in the subsequent steps by the adsorption of an additional H_2O molecule (in an acidic medium) and OH^- (in a basic medium) on the catalyst's active site. It was oxidised next to release the oxygen gas and the original, undamaged active spot of the catalyst.

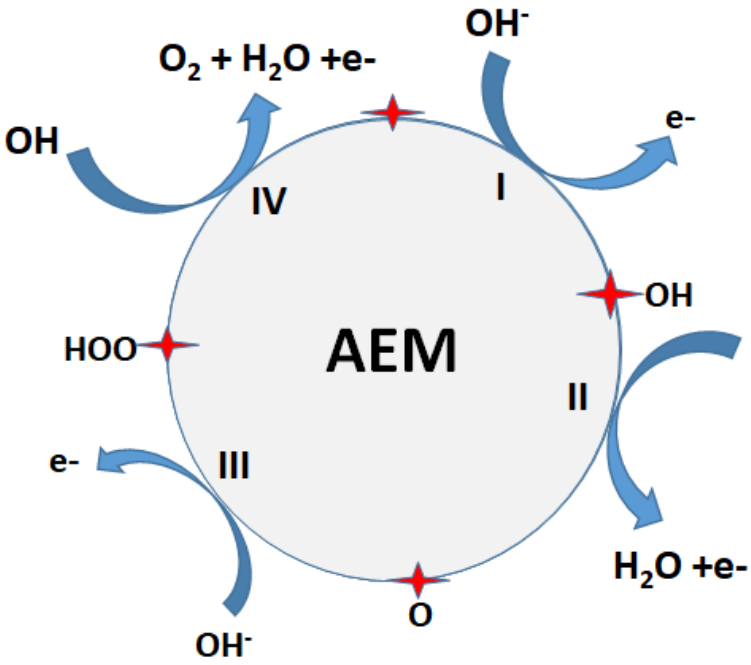

Figure 1.4 OER reaction mechanism based on AEM theory. Here * shows the active site (M) of the transition metal cation and I,II,III and IV corresponds to the four elementary steps involved in the reaction [25].

The reaction-free energies (ΔG) for these steps may be analysed using a theoretical study, density functional theory (DFT) and ideally, any one of these four reaction steps might be used to assess the catalytic activity for OER of a certain electrocatalyst. The four steps reaction-free energies of a perfect OER electrocatalyst should be comparable even in the absence of external bias, but only the application of outside bias can satisfy this

requirement because of the link between the adsorption binding energies of M-OH (E_{M-OH}), M-O (E_{M-O}) and M-OOH (E_{M-OOH}). The slope of E_{M-OOH}/E_{M-OH} is almost equal to 1 and the intercept is 3.2 eV [28]. On the other hand, because M-O is doubly bonded to the surface while M-OH and M-OOH is single bonded, both E_{M-OOH}/E_{M-O} and E_{M-OH}/E_{M-O} show slope close to 0.5 [29]. This correlation of binding energy is prevalent on the surfaces of metals and metal oxide such as rutile, spinels, and pervoskites among others., The binding energy is unaffected by the strength of the surface binding, irrespective of the binding location. The strength of the binding between oxygen and catalyst surface is controlled by the formation of M-OOH and M-OH species. Strongly bonded surfaces yield M-OOH species, whereas weakly bonded surface form M-OH species [28]. As a consequence, a volcano-like relationship forms between the electro-catalytic performance and adsorption energy of oxygen [30]. At the volcano's crest, catalysts have a stable equilibrium of binding energies, which improves OER results. The OER performance of various electrocatalysts can now be correctly described and estimated using this model, which has acquired widespread recognition as a descriptor on a global scale. Moving the difference between the ΔG_{M-O} and ΔG_{M-OH} ($\Delta G_{M-O} - \Delta G_{M-OH}$) closer to the volcano plot's top can optimise and hypothesise the catalytic activity [31].

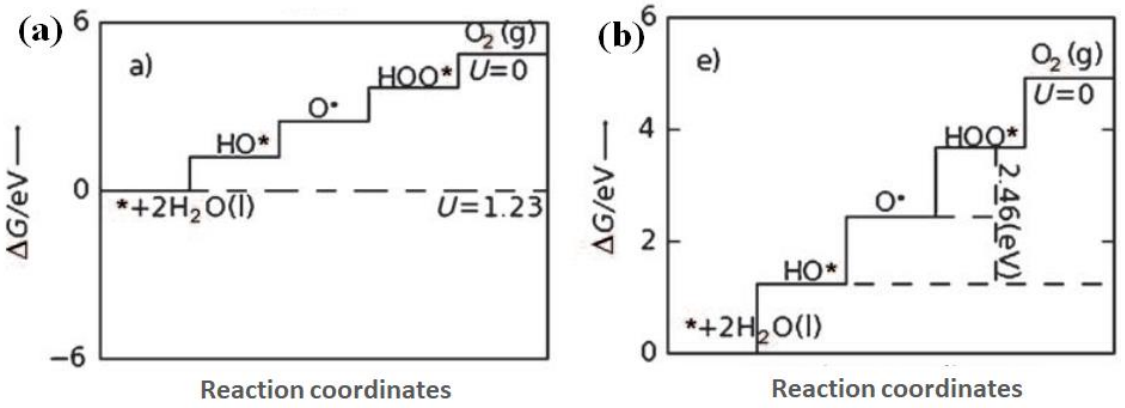

Figure 1.5 Standard free energy plot for the ideal catalyst (a) at zero potential (U=0), equilibrium potential for OER (U=1.23) and (b) at the potential, U = 2.46 V [28].

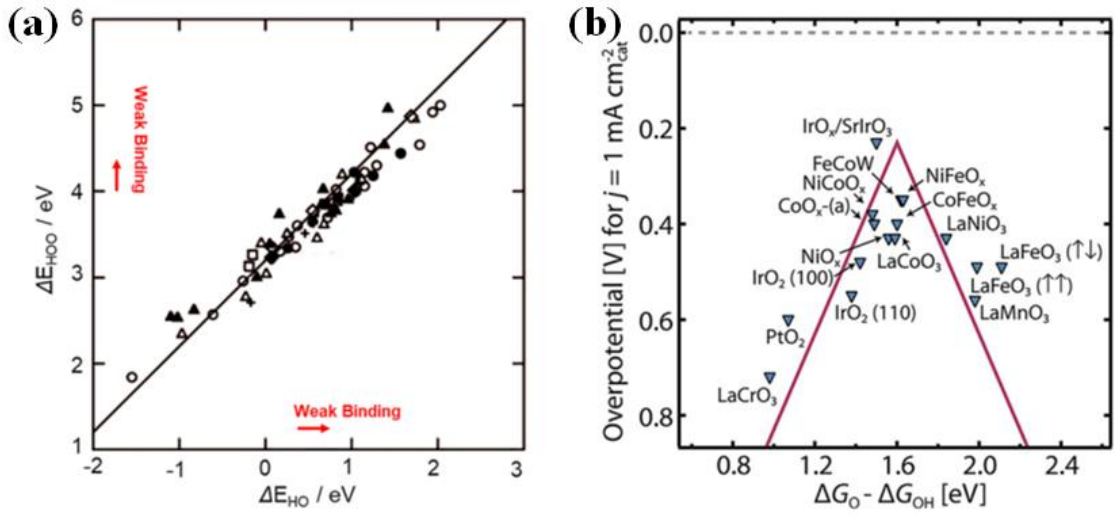

Figure 1.6 (a) A plot of adsorption energies of HOO* and HO* on metal oxides. Hollow symbols represent the adsorption energy on clean surfaces: perovskites (circle), rutiles (triangle), Mn_xO_y (square), anatase (diamond), Co_3O_4 (+). The solid symbols shows the absorption energies on high-coverage surfaces [28]. (b) The volcano relationship between ΔGO*-ΔGHO* and OER activity for oxides [30].

1.3.1.1 (b) Lattice-oxygen-mediated mechanism (LOM)

In this mechanism, the electrocatalyst contains lattice oxygen, and an atom of lattice oxygen is used to produce O_2 gas [32]. In the first step, a water molecule is adsorbed on active sites of the electrocatalyst (M or *) and gives M-OH through the generation of H^+ and e^- pair then this M-OH generates M-O in the second step similar to AEM (an acidic mechanism). The electrocatalyst's lattice oxygen atom and M-O interact in the third step to release one oxygen molecule (O_2) and draw out of a vacancy of oxygen (V_o). A clean

M site is recreated by removing absorbed H^+ from the M-OH in the fourth stage, which also involves further H_2O adsorption and dissociation to produce absorbed H^+ and MOH. The LOM states that the electronic structure of the catalyst is controlled by the bond strength of the oxygen-metal bond, which regulates the OER mechanism of LOM.

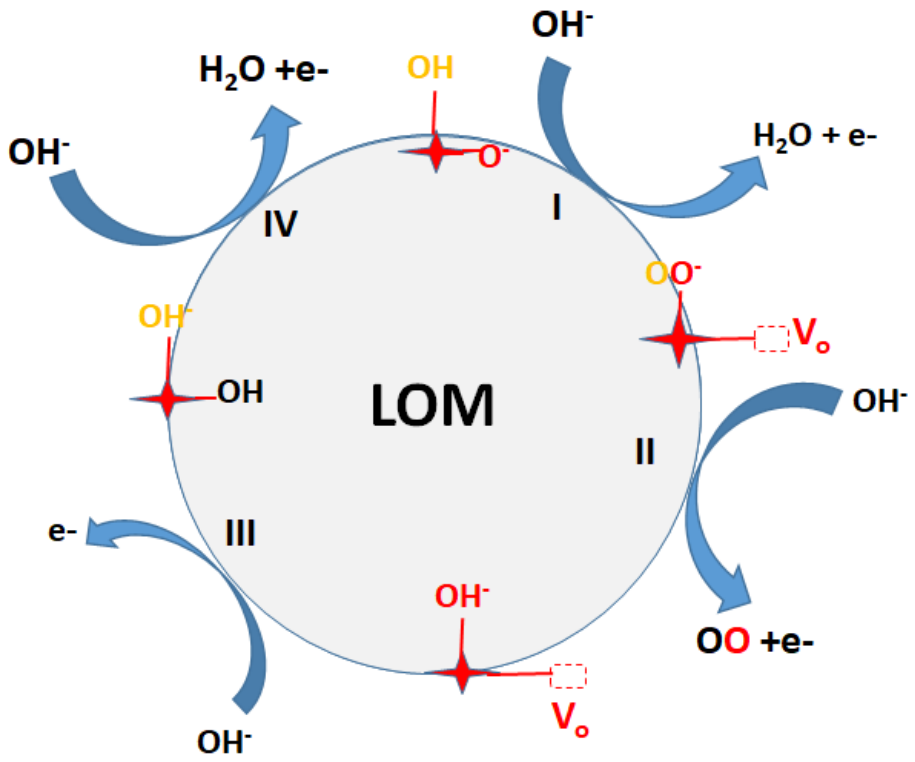

Figure 1.7 Construction of OER cycle path accordingly LOM theory. Here, * represents the active site of the catalyst (transition metal cation) and I, II, III and IV are elementary steps [26].

The mechanism for OER can be guided from Adsorbate evolution mechanism to Lattice oxygen mediated depending on the energy location of d-band of metal and p-band of oxygen in metal oxide. When the energy level of metal's d-band is above than that of the p-band of oxygen, electrons are moved from the d-band to the p-band. Additionally, the metal site also functions as an active centre and adsorption, allowing water to be oxidised using AEM. On the other hand, when the energy levels are switched, ligand holes can be created when electrons from the p-band of the ligand go to the d-band of the metal.

Moreover, by organising their structural elements in a way that requires less energy, these ligand gaps promote the evolution of species that are oxygenated [$(O_2)_n$]. Because of this, it is possible for the OER mechanism to switch from AEM to LOM, and this change in the mechanism may be seen on the reversible hydrogen electrode scale for processes that depend on pH [32, 33].

1.4 Importance of OER in other fields

1.4.1 Metal-air batteries

Lithium-ion batteries (LIBs) have been widely used as an energy source from a long time but their restricted energy density (theoretically, 400 Wh kg^{-1}) limits their application as the energy source for the succeeding generation [34, 35]. In this concern, metal-air batteries have found a promising contender that can fulfil the accrescent demand for high energy density. Metal-air batteries offer inexpensive, environmentally benign power sources for portable electronics and electric vehicles, and they have significant promise for large-scale electricity storage. Instead of the closed system of traditional batteries, they have the distinctive feature of an open cell structure that allows oxygen to be breathed from the surrounding environment as an active cathode material [35]. As a result, the battery's weight is decreased, increasing the metal-air battery's energy density. Metal-air batteries primarily consist of three components: a porous cathode, an electrolyte and a metal anode, all of which extensively utilise the metals Li, Na and Zn [35, 36]. All metal-air batteries have oxygen reduction reactions and oxygen evolution reactions, regardless of the anode material. The electrolyte used determines how these reactions will proceed.

During the ORR, in an aqueous free Li-air battery, Li_2O_2 or LiO_2 is formed at the surface of the catalyst which is insoluble and is drawn to the pores of the air cathode [37]. The

overall reaction can be stated as of the catalyst which is insoluble and is drawn to the pores of the air cathode [37]. The overall reaction can be stated as-

$$2\,Li\,(s) + \,O_2(g) \rightarrow Li_2O_2(s) \quad (E^0 = 2.96\,V) \quad \text{(Eq. 1.23)}$$

$$\text{Or} \quad 4\,Li\,(s) + \,O_2(g) \,\rightarrow\, 2Li_2O \;\; (s)\;(E^0 = 2.91\,V) \quad \text{(Eq. 1.24)}$$

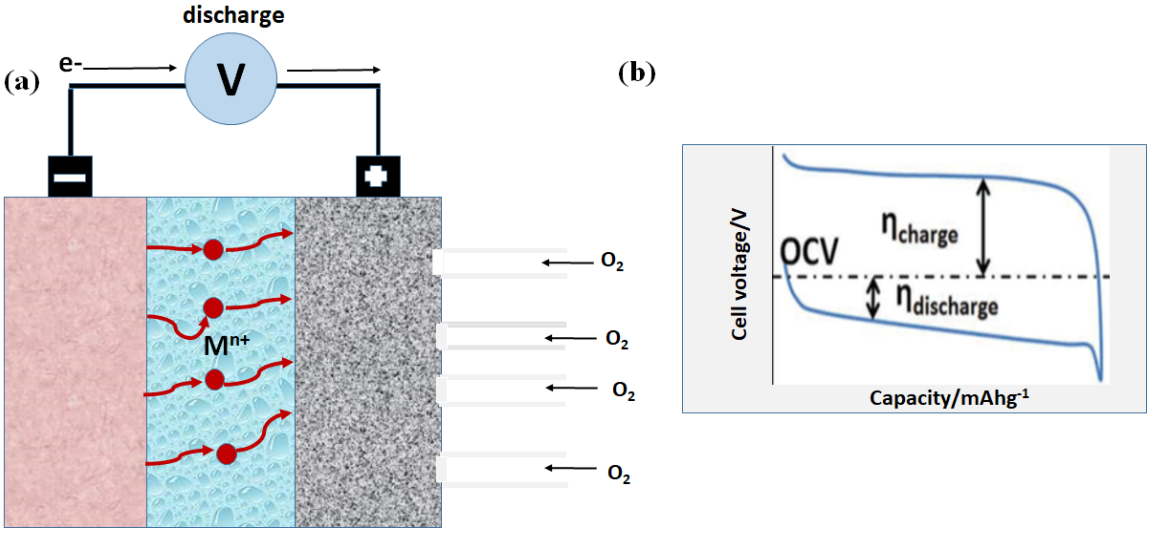

Figure 1.8 (a) Schematic showing the image of a metal-air battery; the metal act as a anode and porous air electrode act as a cathode and, (b) charge discharge curve for metal-air battery [36].

In contrast, the basic aqueous electrolyte used in Li-air batteries causes the formation of LiOH in the course of ORR, which is soluble in the electrolyte and does not obstruct the air cathode's pores during discharging [36]. The reaction can be sketched as-

$$4\,Li\,(s) + \,O_2(g) + \,2H_2O(l) \,\rightarrow 4\,LiOH\,(s)\,(E^0 = 3.2\,V) \text{ (Eq. 25)}$$

Similar to an aqueous Li-air battery, discharging process in the Zn-air battery converts oxygen into hydroxyl ions or hyperoxide ions. In parallel, Zn ions from the anode are discharged, where they interact with hydroxyl ions to form zincate ions [$Zn(OH)_4^{2-}$]. Further, the decomposition of zincate ions results in the formation of zinc oxide (ZnO) [36]. The reaction might be expressed as-

$$Zn\ (s) + \ O_2\ (g) \rightarrow 2\ ZnO\ (s)\ (E^0 = +1.65\ V) \qquad \text{(Eq. 1.26)}$$

The Zn-air batteries are reasonably priced, practical, and have a high energy density. But among all types of metal-air batteries, lithium-ion batteries have the potential to provide the best theoretical density in response to high potentials. Despite these advantages, the performance and durability of Zn-air and Li-air batteries still have a number of drawbacks, including as low power density, susceptibility to airborne contamination, and evaporation of the electrolyte because of their open cathode designs.

Key performance indicators for any metal-air battery are the rate of charge-discharge, capacity preservation, energy effectiveness, and cycling lifetime. These indicators are all primarily controlled by two processes, oxygen reduction and oxygen evolution. These two reactions occur at discharging and charging of the metal-air battery. The most common discharge-charge curve of a MAB is depicted in Figure 1.8(b). The power output and efficiency across a full cycle of metal-air batteries are severely constrained by the overpotentials of both processes, ORR ($\eta_{discharge}$) and OER (η_{charge}).

In the air electrode of the metal-air batteries, there are various processes related to the ORR process. The O_2 is first diffused to the surface of the catalyst from the surrounding atmosphere. Then, the oxygen molecules receive electrons from the anode, which weakens the O=O bond, and hydroxyl ions are subsequently eliminated as a by-product from the surface of the catalyst to the electrolyte (in a non-aqueous Li-air battery, the solid product is formed). While the OER process when a metal-air battery is being charged, it follows the reverse process of ORR. The activity and morphology of the catalyst as well as the structural layout of the air cathode all influence how well the air electrode performs in a MAB.

There have been significant efforts made to develop the ORR catalyst with high activity in recent times [37, 38], but there are still a great deal of real-world issues and underlying problems that need to be clarified. Several studies shows that the employment of catalytic active materials in air electrode can significantly reduce the overpotentials for both the processes [39-41]. Therefore, understanding the detail mechanism of ORR and OER is essential to successfully design efficient catalyst material for both processes.

Noble transition metals and their alloys are too costly to be practical for large-scale applications even if they have excellent electrocatalytic performance for ORR and OER. Therefore, it is necessary to develop catalysts that are both affordable and practical for metal-air battery.

1.4.2 Fuel cell

An electrochemical cell known as a Fuel cell which provides a framework for producing green and clean energy without endangering the environment. It converts the chemical energy of a fuel (H_2) and oxidising agent (O_2) into electricity through two redox reactions. Batteries also convert chemical energy into electrical energy. Contrary to most batteries, though, fuel cells always have fuel available, and oxygen is used to keep the chemical reaction going. Batteries, on the other hand, use the chemical energy that is already contained in the battery's components. The first fuel cell was discovered by Sir William Grove in 1838, and after more than a century, Thomas Bacon's hydrogen-oxygen fuel cell (also known as an alkaline fuel cell) was developed in 1932 [42]. The *NASA Apollo* mission used the alkaline fuel cell, commonly referred as the Bacon fuel cell, to supply water and electricity to the crew.

Anode, cathode and electrolyte are the components of a fuel cell, and hydrogen ions (H^+) or hydroxyl ions (OH^-) are transferred between the two sides. H_2 is oxidised at the anode

through the hydrogen oxidation reaction (HOR), while O_2 is reduced at the cathode via oxygen reduction reaction (ORR). The reaction in the fuel cell is described as follows-

Reaction at the cathode: $$O_2 + 2H_2O + 4e^- \rightarrow 4OH^-$$ (Eq. 1.27)

Reaction at the anode: $$2H_2 + 4OH^- \rightarrow 4H_2O + 4e^-$$ (Eq. 1.28)

Overall cell reaction: $$2H_2 + O_2 \rightarrow 2H_2O$$ (Eq. 1.29)

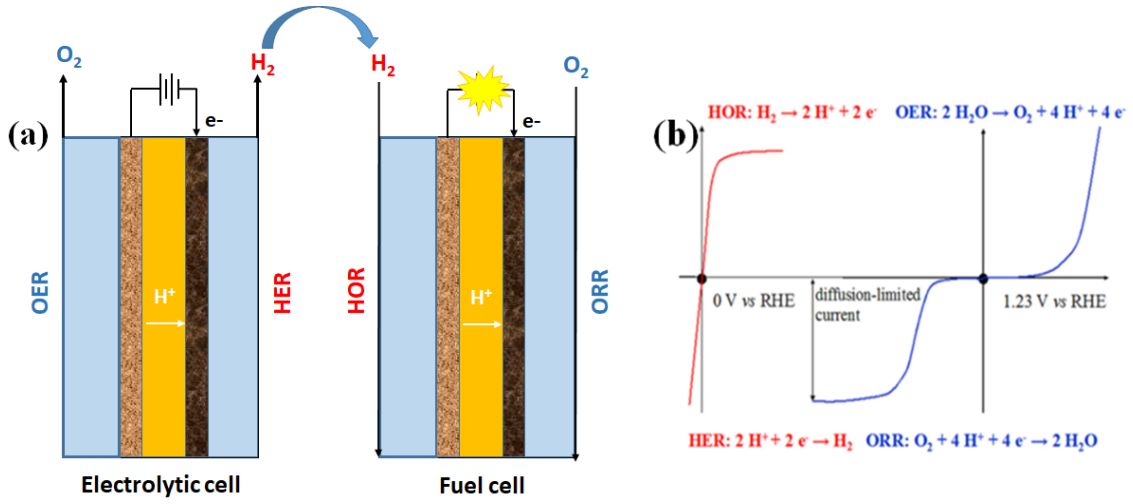

Figure 1.9 (a) Diagrammatic illustration of the electrolytic cell and fuel cell and, (b) polarization curves related to the hydrogen involving reactions (presented as red curves) and oxygen involving reactions (shown in blue curves), respectively [43].

Depending on the electrolyte and the fuels used, varieties of fuel cells are made such as molten carbonate fuel cells, solid oxide fuel cells, alkaline fuel cells, polymeric electrolyte membrane (PEM) fuel cell and phosphoric acid fuel cells. Among these, solid oxide fuel cells are highly efficient (theoretical efficiency~ 85%) and relatively cost-effective but their high operating temperatures (between 800 to 1000 ℃) limit their applications [42].

Intermittent energy storage and conversion with reduced cost and increased energy density are perceived for the continuous power supply. Reversible fuel cells (RFCs), a unique idea that takes this into account, combine a fuel cell with an electrolyzer similar

to rechargeable battery. They have a larger theoretical specific energy (3660 Wh/kg) and a specific energy (400-1000 Wh/kg), which is almost five times higher than batteries. [43]. Reversible fuel cells can be operated using either the fuel cell approach or the electrolyzer approach. In RFCs, the fuel cell mode efficiently and sustainably converts the chemical energy of a fuel (H_2) and an oxidant (O_2) into electrical energy and water. While electrolyzer mode stores the electricity by splitting water into H_2 and O_2. When creating power and storing it in chemicals using electricity, the fuel cell and electrolyzer modes are comparable to the emptying (discharging) and filling (charging) phases of a battery. The oxygen electrode must be stable and active since it functions as the cathode in a fuel cell and anode in an electrolyzer, respectively, and is accompanied by oxygen reduction and oxygen evolution reactions.

Since several applications involve moving from the fuel cell cathode for the ORR to the anode for the OER in the electrolyzer, it is necessary to design dual-purpose catalysts that ate simultaneously active for ORR and OER [44]. Theoretical studies show that no single active site is skilled for catalysing both ORR and OER simultaneously [45] which presents a major obstruction in the electro-catalysis society. For instance, while Pt-based catalysts are thought to be state-of-the-art for ORR, they are not a viable alternative for OER when operating in the high potential window because Pt oxides accumulate at the surface and reduce the catalyst's activity. Due to their high activity, stability and superior electrical and ionic conductivities, Ir and Ru oxides are the most effective and stable catalysts for OER, but because of their ineffectiveness for ORR, they cannot be used as a bifunctional catalyst [46].

1.5 Emerging electrocatalysts for OER

IrO_2 and RuO_2 are the most securitized materials and are regarded as the benchmarking catalysts for OER owing to their distinguished catalytic properties towards OER. However, these materials' high cost and inadequacy as well as their low electrochemical stability (especially for Ru) hinder their use in commercial applications. During the mechanism, they degrade through the conversion of Ru^{4+} and Ir^{2+} into $[Ru^{8+}]\ O_4$ and $[Ir^{6+}]\ O_3$ species respectively, which are dissolvable in an aqueous solution [47]. With respect to these materials, non-noble transition-metal oxides have drawn considerable attention for OER because of their cost-effectiveness, plenty in nature and significant electrocatalytic performance. Due to their several oxidation states, these materials are regarded as ideal prospects for OER. Their catalytic performance is significantly influenced by factors such as their morphological structure, arrangement, oxidation states, the surface oxygen binding energy and the d-electron density of the transition-metal ions. In the past few years, the most studied materials comprised spinels, perovskites, transition metal-oxides, layered double hydroxides, chalcogenides, pnictides and metal-organic frameworks [7, 48-50] which are compressively detailed in the following subsections.

1.5.1 Spinel catalysts

The spinel structure is a form of AB_2O_4 structure, where A is Mn, Cu, Fe, Ni, Co, Zn, and B is Co, Fe, Ni, and Mn, and O is an oxide ion (O^{2-}) .O^{2-} ions are organised in cubic close-packed (ccp) lattice, and tetrahedral and octahedral positions are occupied by the A^{2+} and B^{3+} cations, respectively. If the crystal field stabilisation energy (CFSE) of B^{3+} in the octahedral site is greater than the CFSE of the A^{2+} in the octahedral site then it will be normal spinel and all A^{2+} occupy the tetrahedral site and all B^{3+} occupy the octahedral site. In contrast to it, if the CFSE is reversed, then it will be the inverse spinel, A^{2+} goes to the octahedral site and half of B^{3+} resides in the tetrahedral and octahedral sites. Several

spinels can be made by varying transition metals in cations A and B. These materials gained much interest, particularly Co_3O_4, due to the appropriate adsorption affinity for hydroxide anion [51, 52]. Still, their low surface area and poor conductivity are challenging in electrochemical conditions. Yanguang Li et al. show that doping of Ni and Fe in Co_3O_4 can further enhance electrical conductivity [53].

A recent study by Xu et al. looked into the possibility that plasma treatment of bare Co_3O_4 results in a high concentration of oxygen vacancies, which is what causes the increased the performance of OER. The overpotential and Tafel slope for this catalyst are 300 mV (at 10 mA cm^{-2} current density) and 68 mV dec^{-1}, respectively [54]. Furthermore, the Gao et al. group succeeded in synthesising hollow microcuboids structured $NiCo_2O_4$ in order to study the impact of surface area, conductivity and electrolyte diffusion on the surface of the catalyst.

The hierarchical hollow structure furnishes a high surface area that provides an easy path for the diffusion of electrolytes (OH^-), showing higher activity for OER and HER [55].

During the electrochemical conditions (OER), the catalyst surface went through various intermediates formation and changed very differently from the bulk material. The surface experience phase transformation in the large anodic environment in the vicinity of the reactants and the surface oxides transformed into the highly active oxyhydroxide species [56]. According to Tung et al., coating of Co_3O_4 nanocubes with a thin layer of CoO produces enduring stability for 1000 hours, which is the longest duration for OER to date. This coating also results in a highly efficient OER performance with an overpotential of 430 mV at 10 mA cm^{-2} with Tafel slope 89 mV dec^{-1} [57]. Later, examined with the “In situ grazing angle X-ray diffractometry” characterization technique, they revealed that the active species, oxyhydroxide phase formation is mainly due to the CoO layer, which is very facile in developing the oxyhydroxide phase [58]. Later, these oxyhydroxide

active species motivated the researchers to create layered hydroxide materials for oxygen evolution application, which will be discussed later in the upcoming subsections.

Experimental observations proposed that in spinel, the redox-active octahedral site has more contribution than the tetrahedral site towards OER and the electronic structure of octahedral-occupied transition metal is recognised as the activity descriptor [59]. Figure 1.10 shows the volcano plot in which the OER activities of spinels are plotted with respect to the e_g occupancy of octahedral cation, signifying that the eg filling of octahedral cation governs the binding strength of OER intermediates. While, for tetrahedral, the plot of OER activities versus e occupancy does not reveal a clear pattern, recommending that the tetrahedral geometry has not significant contribution towards OER [60, 61]. Further, this is validated through the comparison of the activity of spinels $ZnCo_2O_4$ and Co_3O_4. Both spinels exhibit normal spinel structures.

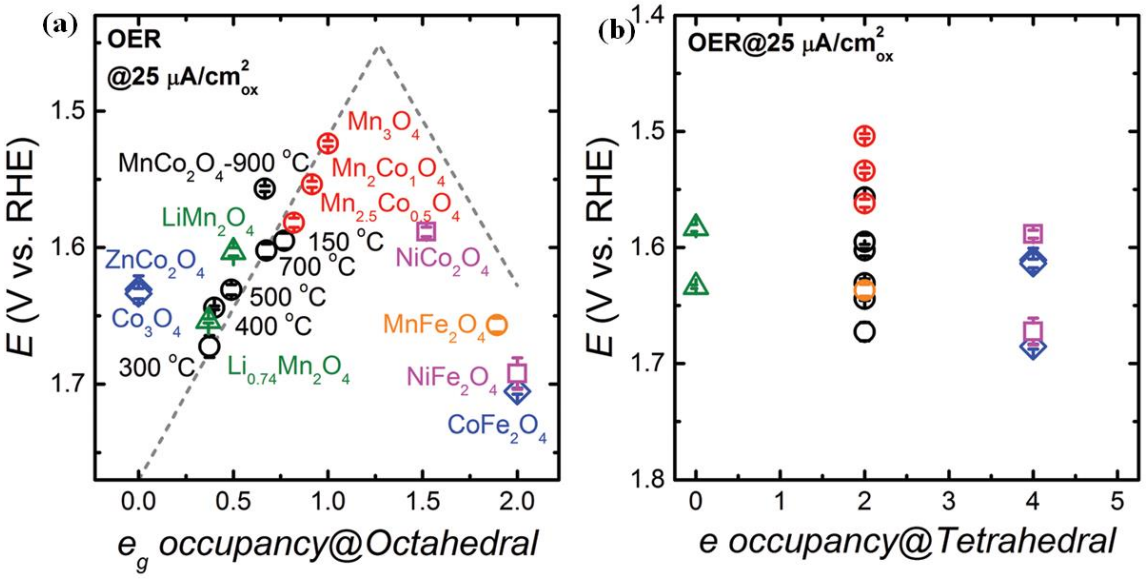

Figure 1.10 Plot of the OER activities of the spinels with respect to the (a) e_g occupancy of octahedral cation and (b) e occupancy of tetrahedral cation [61].

X-ray absorption fine structure (EXAFS) demonstrates that in $ZnCo_2O_4$, the catalytically inert Zn occupy the tetrahedral site and all Co occupies the octahedral site whereas, in Co_3O_4, Co occupies both the tetrahedral and octahedral site. Both the spinel have

comparable OER activity because in both the octahedral composition (Co^{3+}) is the same the only difference is due to the tetrahedral composition (Zn^{2+} versus Co^{2+}) indicating that Co^{2+} in the tetrahedral site does not contribute OER significantly [62, 63]. Moreover, a series of metal-substituted cobaltite spinel oxides MCo_2O_4 (M = Ni, Zn, Mn, etc.) is also studied for OER, which suggests that Co occupying the octahedral site is critical for high OER performance [64].

1.5.2 Perovskites, Layered double hydroxide (LDH) and Other non-noble metal-based catalysts

The substances known as perovskites have the general formula ABO_3, where A stands for alkaline-earth or rare earth metals, B for transition metals, and O for oxygen. They are constitutionally analogous to the spinels and arranged in a cubic-symmetry structure with 12-fold oxygen coordination of A and 6-fold oxygen coordination of B. They appeared as a significant class of functional materials due to their low-cost and earth-abundant composing elements. Their effectiveness in OER reactions has been known for a long time and through the partial substitution of cations at A, B or both A and B sites, with the formula $A_{1-x}A'_xB_{1-y}B'_yO_{3-\delta}$, a diversity in perovskites can be generated having flexible physical and chemical properties [48, 65, 66].

Compared with perovskites and spinels, transition-metal oxides and hydroxides such as CoO, NiO, Ni-Fe LDH, Co-Ni LDH etc. possess a lesser probability of tuning the electrical properties [67, 68]. Still, they are eye-catching contenders for OER because their easiness in synthesis and nanostructure formation offers a large surface area. These oxides and hydroxides are speculated as good OER catalysts because their structure resembles the oxyhydroxide intermediates, formed on the surface of the spinel in the course of OER. Moreover, in these oxides, uncommon metal oxidation states are

generated due to the oxygen defects which facilitate fast charge transfer for OER intermediates with optimum adsorption energies [69].

The OER performance of transition metal chalcogenides and pnictides is also comparable to that of oxide materials [68]. Their substantial OER activity is caused by the growth of oxygen-containing species, such as oxide or hydroxide layers, on the surface by the chemical transformation in anodic [70, 71]. Although it is unknown what causes their high activity, the majority of OER active materials in chalcogenides and pnictides materials are composed of Ni- and Co-based compounds. This may be connected to how easily oxide layers grow on the surface. For instance, Jun Song Chen et al. demonstrated effective OER activity with an overpotential of ~300 mV at 10 mA cm^{-2} in NiS nanosheet arrays supported on a stainless steel mesh [72]. Due to the larger size of anions that make doping at the metal site simple, other metal-chalcogen bonds, as opposed to oxides, are weaker and more covalent. As a result, the catalytic activity can be easily changed by utilising various metal-to-chalcogen ratios as well as doping at the metal site. Furthermore, Stern et al. made the first proposal for nickel pnictide (Ni_2P) surface oxidation. It changes into a Ni_2P/NiO_x core-shell assembly structure during the course of the reaction, and this structure exhibits OER performance with an overpotential of 290 mV at 10 mA cm^{-2} and Tafel slope of 59 mV dec^{-1} as well as stability for 10 hours [73]. The performance and stability of Co-based compounds such as CoP, $Li_2CoP_2O_7$, $Na_2CoP_2O_7$, $NaCoPO_4$ and $LiCoPO_4$ are also rather good [74, 75].

1.5.3 Metal-organic frameworks (MOFs): a promising OER electrocatalyst

Among various emerging electrocatalysts, metal-organic framework (MOF) shows great potential, and over a couple of decades, these have been developed as promising materials for extensive applications in industry and society. MOFs are a class of porous crystalline materials made up of inorganic metal ions or metal clusters (known as nodes) and organic

ligands (called linkers) through the linkage of coordination bonds [76, 77]. Due to inorganic metal ions or metal clusters (also known as a secondary-building unit or SBU) and an organic molecule, MOFs are frequently mentioned as hybrid inorganic-organic materials. MOF lattices can be designed with known geometries and coordination environments via the spontaneous self-assembly of simple molecular building units, and their crystal structures can be altered from 3D structures to 2D layered structures, which provides a new aperture to tune up the various structure-property relation between the junction of hard and soft inorganic and organic materials.

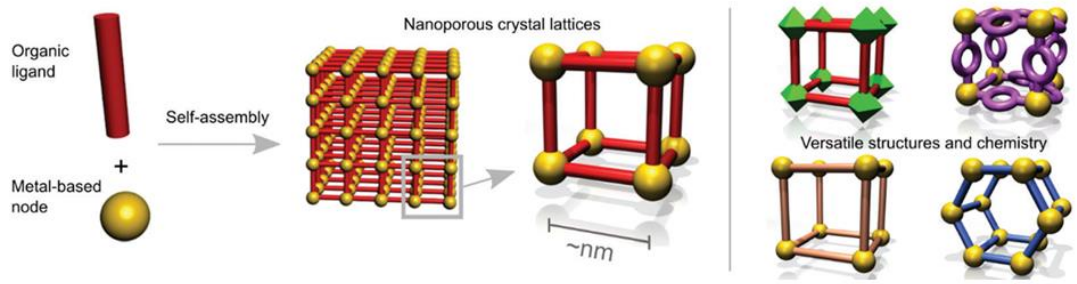

Figure 1.11 Schematic representation of the synthesis of MOF with organic ligand and metal node and their structural and chemical versatility for various applications [78].

In electrocatalysis, MOFs emerged as fascinating materials for water splitting and fuel cell applications due to their flexibility in structures, short and long-range order, large surface-area and intrinsic porosity with pores of tunable size [78-81]. They also act as precursors or templates for synthesising porous carbons and metal oxide nanoparticles. The synthesis of porous carbon using MOF as a precursor was first described by the Bo Liu et al. group in 2008 [82] and the carbonization (pyrolysis) of MOFs was extensively accepted as an efficient approach to derive carbon-based nanomaterials with various morphologies and compositions [83]. These carbon-based nanomaterials obtained from MOFs show potential applications in energy conversion and storage, endowing

interesting features such as the regulation of the morphology and porosity to expose the active sites and facilitate the mass transport and the good distribution of metal species in

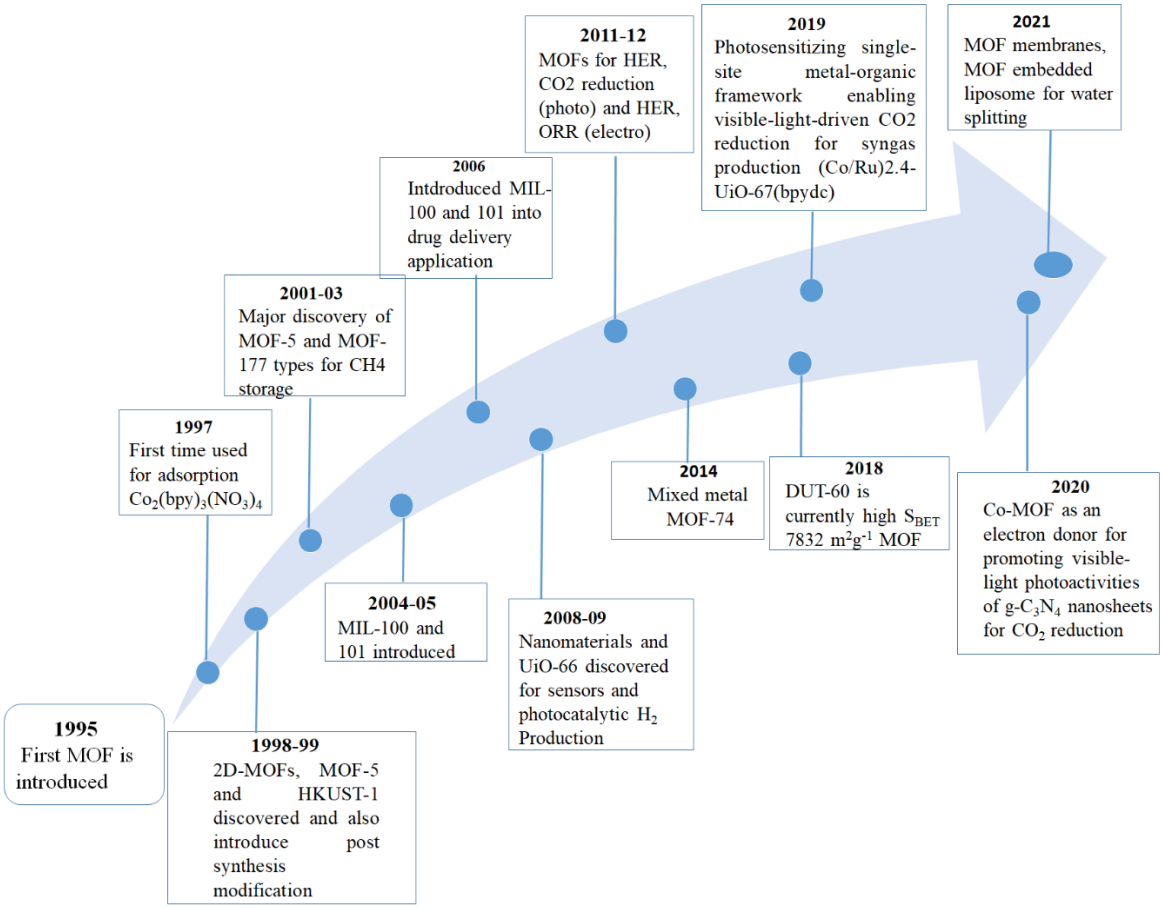

Figure 1.12 A roadmap of MOFs materials from the past to present.

carbon material improving the efficiency of electrocatalytic reactions. Moreover, the catalytic performance of the carbon-based nanomaterials can be further enhanced with doping with heteroatoms (like N, S, P etc.) and heteroatoms containing organic ligand act as the self-dopant, for example, DTO (dithiooxamide) which is a dual heteroatom (N and S) doped organic ligand. Because of the difference in electronegativity and spin density between heteroatoms and carbon, charge polarization occurs which assists their performance [84, 85]. Besides, adding other materials such as metals, metal oxides or other nanoparticles into these heteroatom porous carbons amplify the conductivity of as-designed hybrid materials [86, 87]. For instance, Shweta et al. showed that the OER

performance of N/S doped porous carbon (NSC), derived from the zinc dithiooxamide metal-organic framework (ZnDTO MOF), enhanced eight times after the physical mixing with Co_3O_4 because of the greater conductivity of composite material [88]. Moreover, varieties of MOFs and MOF-based materials are used by different groups for various applications in which few are listed in Table1.1

Table 1.1 MOFs and MOF-based materials for various applications.

S.No.	MOFs/MOF-based Materials	Electrolyte	Application	References
1.	Ce-MOF	KOH	OER	[89]
2.	Cu-MOF	H_2SO_4	HER	[90]
3.	C-Zn/Co ZIFs	NaCl	CO_2 hydrogenation	[91]
4.	Ti/TiO2 NT-ZIF-8	Na_2SO_4	CO_2 reduction	[92]
5.	ZnO@ZIF-8	Phosphate buffer	Sensor	[93]
6.	CoNi-MOF arrays	KOH	Supercapacitor	[94]

Another type of MOFs are Prussian blue analogues (PBAs). These are a class of three-dimensional metal-organic framework materials made up of cyanide ligands and various transition metal cations. In this framework, transition metals are bonded through cyanide-bridging ligands in a cubic crystal structure. In fact, PBAs are derived from Prussian blue (PB) which is an ancient pigment, discovered in the 18^{th} century. It contains Fe^{3+} and Fe^{2+} metal ions, bridged by the cyano group having the formula $Fe_4[Fe(CN)_6]_3$ in a three-

dimensional framework structure with a cubic crystalline unit [95]. Putting the other transition metals such as cobalt, nickel, copper, zinc and manganese in the place of iron, numerous PBAs can be created with discrete compositions and similar crystal structures. Their low-cost, easy synthesis method and tuneable composition make them potentially applicable in many fields, such as biosensors [96], electrochromic displays [97], rechargeable batteries [98], fuel cells and electrocatalysis [99-102]. Among these, PBAs are more attractive and most promising for electrocatalysis towards water splitting [103]. Further, these PBAs can be converted into functional metal oxides, carbides, sulphides and phosphides holding their original nanostructures [102, 103]. Apart from this, PBAs can be transformed into open-cage/frame-like nanostructures, a particular class of these complex materials. In electrocatalysis, the open structures are viewed as more advantageous than the solid counterparts because the open constructions exhibit high surface-to-volume ratios with respect to conventional shape, which facilitates the contact of electrolyte with electrocatalyst resulting the enhanced electrocatalytic performance [104]. For example, the Chen et al. group showed a highly open-framework structure of Pt_3Ni rhombic dodecahedral for ORR [105] and the Jianwei Nai et al. presented a metal selenide open nanocage derived from the Ni-Fe PBA nanocubes for the enhanced OER performance [104].

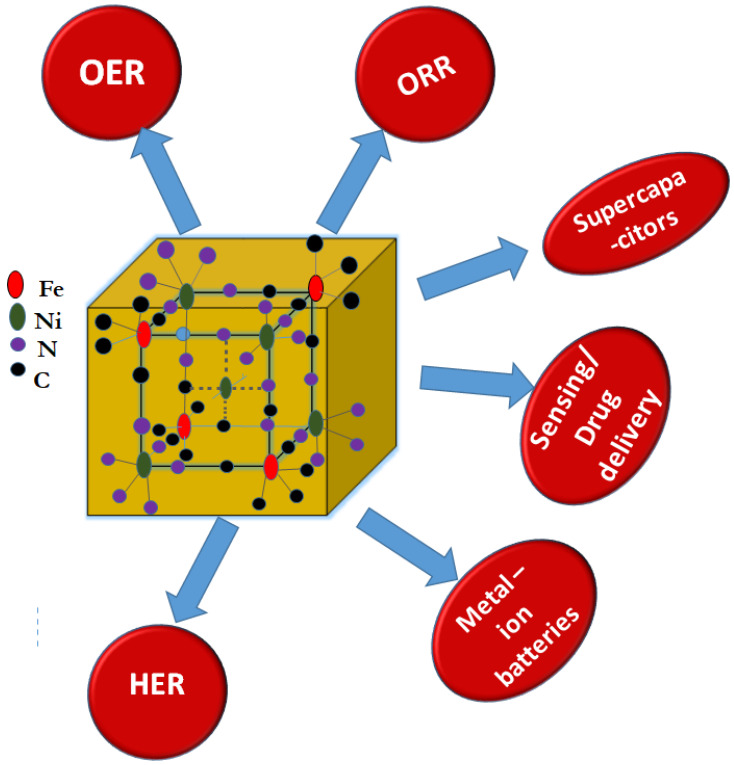

Figure 1.13 The unit cell structure of Ni-Fe-PBA. Fe^{III}, Ni^{II}, C and N are represented by red, green, purple and black, respectively and applications of PBAs and their derivatives in various fields [106, 107].

1.6 Evaluating parameters for OER activity

The catalyst is an imperative and first prior component for the good performance of any reaction, but the selection of appropriate electrolyte and specific kinetic parameters for instance, over potential, Tafel slope, electrochemically active surface (ECSA) etc., have significant importance in understanding and interpreting the mechanism of any reaction. A detailed description of these parameters is listed in the subsequent subdivisions.

1.6.1 Electrode and electrolyte

The working electrode and electrolyte are important parts of ascertaining the good performance of the reaction. The reaction rate is greatly affected by the structures, conductivity and degree of wettability of the working electrode/substrate. Based on the surface structure and movement of the electrolyte, there are two types of electrode supports, the first is a flat surface and the other is a 3D electrode. Glassy carbon (GC),

Cu/Ti foil and indium-doped tin oxide (ITO) substrates are flat surface electrodes, which permit one-sided diffusion of electrolytes whereas, 3D substrates like carbon cloth (CC), carbon paper (CP) and Ni foam provide multiple paths for electrolyte access from all sides of catalysts.

Electrolytes substantially impact the performance of the electrode material, and the activity of the catalyst varies differently in different electrolytes. An alkaline medium is more supportive for OER, while in the neutral electrolyte, it is a challenging process, and in the acidic medium, it has very poor performance. The search for stable electrocatalysts in alkaline conditions is given the utmost priority. Maximum efforts are dedicated to searching the stable electrocatalysts in alkaline circumstances. Carbon-based materials, oxides or oxy-hydroxides of transition metals, hybrids, spinels, perovskites and metal-organic frameworks (MOFs), are highly stable electrode materials in alkaline medium but in acidic conditions; many of these materials are not entirely stable because of high oxidation potential. Therefore, it is highly anticipated to look for an OER electrocatalyst that can work under a wide range of pH (0-14).

1.6.2 Onset/ Overpotential (η)

Onset potential is the most important aspect of gauging the OER performance of catalysts. It is difficult to spot the precise value of onset potential; therefore the value of the potential at a specified current density is considered to assess the performance of catalysts. Comprehensively, 10 mA cm^{-2} (i_{10}) is taken as the specific current density and the value of the potential at this current density is termed as the overpotential (η_{10}). Overpotential is described as the difference between the electrode potential (E) and equilibrium potential, E_{eq} (1.23 vs. RHE) of the electrode reaction. Eq. 1 illustrates the Nernst equation given as follows-

$$E = E^0 + \frac{RT}{nF}\, ln\frac{C_O}{C_R} \qquad \text{(Eq. 1.30)}$$

Where E is the real applied potential, E^0 is the standard electrode potential, R is the gas constant (8.314 $JK^{-1}mol^{-1}$), T is the absolute temperature, n is the number of transferred electrons in a battery reaction, C_O and C_R is the concentration of oxidised and reduced species, and F is the Faraday constant (96485.33 s A mol^{-1}), respectively.

Overpotential is given as below-

$$\eta = E - E_{eq} \qquad \text{(Eq. 1.31)}$$

Generally, overpotential is taken in mV; for example, if a catalyst reaches 10 mA cm^{-2} current density at 1.53 V vs. RHE, its overpotential is 300 mV. For a better catalytic activity of the catalyst, the value of the overpotential should be low. If a catalyst holds an overpotential in the range of 300-400 mV, it is put on the list of outstanding catalysts for OER.

1.6.3 Exchange current density (i_0) and Tafel slope (b)

Exchange current density and Tafel slope are the other two fundamental descriptors to evaluate the electrochemical performance of the catalyst. The exchange current density reveals the intrinsic efficiency of the catalyst and it is related to the transfer of electrons between the electrode and the electrolyte. Tafel slope describes the reaction kinetics and mechanism [108]. Generally, any electrochemical reaction comprises of two half-reactions at the cathode and anode, respectively. The reaction that occurs at the cathode is called the cathodic reaction and the reaction occurring at the anode is called the anodic reaction. Therefore, the total current (j) is the sum of the anodic (i_a) and cathodic (i_b) current given as:

$$j = j_a + j_c \qquad \text{(Eq. 1.32)}$$

When the reaction is at the equilibrium, i.e., E = E_{eq}, (Eq. 1.31) then the value of η = 0. Therefore, in that situation, the absolute values of the anodic and cathodic currents are equal to each other, resulting in the net current being zero without net electrolysis. Thus the exchange current density (i_0) is defined as the value of the current in the absence of net electrolysis and at zero overpotential. It is given as the quotient of the current j_0 (magnitude of the intercepts when the reaction is at equilibrium) and the geometric area of the electrode (s) as below –

$$i_0 = \frac{j_0}{s} \qquad \text{(Eq. 1.34)}$$

A higher value of i_0 resembles a better electrocatalyst and electrochemically its magnitude cannot be achieved but using the Tafel equation, we can calculate its value. Butler-Volmer equation also known as the Erdey-Gruz-Volmer equation given in the following (Eq. 1.35) defines the relationship between the current density and the voltage difference between the electrode and electrolyte consisting of cathodic and anodic reactions both.

$$i = i_0 \{\exp\left[\frac{\alpha_a\, n\, F}{RT}\left(E - E_{eq}\right)\right] - \exp\left[-\frac{\alpha_c\, nF}{RT}\left(E - E_{eq}\right)\right]\} \qquad \text{(Eq. 1.35)}$$

$$or,\ i = i_0\,[\exp(\frac{\alpha_a nF\eta}{RT}) - \exp(-\frac{\alpha_c nF\eta}{RT})]$$

$$or,\ i = i_0\,[\exp(\frac{\alpha_a nF\eta}{RT}) + \exp(\frac{\alpha_c nF\eta}{RT})] \qquad \text{(Eq. 1.36)}$$

Where, i_0 is defined as the exchange current density, α_a and α_c indicate the charge transfer coefficients for anodic and cathodic reactions, respectively. Representation of the parameters for n, F, E, R, and T are the same as used in Eq. 1.30.

Further, Eq. 1.6 can be simplified into Eq. 1.7 given as-

$$i \approx i_0 \, exp \frac{\alpha_a nF\eta}{RT} \qquad \text{(Eq. 1.37)}$$

Because at a high positive potential, the overall current is due to the anodic current and the contribution of the cathodic current is almost zero. Therefore, the reasonable presentation of the Butler-Volmer equation can be illustrated as Eq. 1.37 which is the well-known Tafel equation. Moreover, the Tafel equation [108] in Eq. 1.37 can be simplified further using the logarithm function given as follows-

$$logi = logi_0 + \frac{\alpha_a nF\eta}{RT} \log(e) \qquad \text{(Eq. 1.38)}$$

$$logi = logi_0 + \frac{\eta}{b} \qquad \text{(Eq. 1.39)}$$

As α_a, n, η, F, R and T are constants. Thus, the value of $\frac{2.303\ RT}{\alpha_a F}$ can be written as a constant *b* (Tafel slope) and Eq. 1.39 can be transformed into Eq. 140 as follows-

$$\eta = a + b \log(i) \qquad \text{(Eq. 1.40)}$$

Where, $a = \frac{2.303\ RT\ logi_0}{\alpha_a F}$ and $b = \frac{2.303\ RT}{\alpha_a F}$

From the equation, it is evident that the relation between the *b* and η is proportional, and it is inversely related to *i*, indicating that a lower value of *b* gives a smaller overpotential, showing the better catalytic performance of the catalysts. Actually, the Tafel slope is a better tool for recognising the rate-determining step in the range of onset overpotential [108]. For instance, if the value of the Tafel slope is approximately 120 mV dec^{-1} then the first step in the OER mechanism will be the rate-determining step which is a one-electron transfer step. If the second step is the rate-determining step then the Tafel slope will be around 60 mV dec^{-1}, and the value of about 40 mVdec^{-1} corresponds to an electron-proton

reaction. Further, for the third and fourth steps, the conditions become more complex in the prevailing models [109].

1.6.4 Electroactive surface area (ECSA)

The catalytic activity of the catalyst is usually presented in current density, normalized by the geometric area of the electrode. The current can also be normalized through the surface area of the catalyst material. The surface area can be measured through the microscopic (atomic force microscopy) techniques used for non-porous materials and gas adsorption techniques (nitrogen or hydrogen adsorption) used for materials with high surface areas, respectively. Although these techniques are widely important in assessing the surface area of diverse materials, however, they are incapable of differentiating electrically conductive constitutes from non-conductive ones and also the section of the surface which are accessible and not accessible to the electrolyte [110,111]. In that way, an electrochemically active surface (ECSA) is viewed as an appropriate tool to relate the different structural properties of the catalysts with electrochemical perception.

The ECSA of the catalyst can be calculated through the relation of the double-layer capacitance (C_{dl}) and the specific capacitance (Cs) given below [111] -

$$ECSA = \frac{C_{dl}}{C_s} \qquad \text{(Eq. 1.41)}$$

C_{dl} can be measured through either cyclic voltammetry (CV) for direct current (DC) or electrochemical impedance spectroscopy (EIS) for alternating current (AC). Through the EIS method, the value of C_{dl} can be determined using the equation [112]-

$$C_{dl} = Y_0[R_s^{-1} + R_{ct}^{-1}]^{n-1} \qquad \text{(Eq. 1.42)}$$

Where R_s is the solution resistance, R_{ct} is the charge transfer resistance parallel to the constant phase element (CPE). $Y_0(mS.s)$, and n (dimensionless) are the coefficient and exponent of CPE, respectively.

To determine the C_{dl} from CV, first, select a non-faradic region in which no redox reaction takes place; then CV is run with various scan rates and a rectangular shape CV plot is obtained. The slope (divided by 2) of the linear equation; the difference between the anodic and cathodic current density versus scan rates gives the value of C_{dl}. A higher value of C_{dl} corresponds to a higher ECSA. Comparing the catalytic activity of the different catalyst materials under different conditions is a tough task because of the different electrochemical reactions for different materials. However, gauging the performance of a series of similar catalyst materials in the same condition is easier and more reliable.

1.6.5 Stability

In electrochemistry, in addition to the superior activity, exceptional stability is also another important metric for considering the good quality of catalysts. For any catalysts to be applicable on a large scale, it is a very crucial aspect of the electrochemical world. To calibrate the stability of electrocatalysts, three measurements are customarily used often; cyclic voltammetry (CV), chronoamperometry (current versus time graph at a fixed potential) and chronopotentiometry (potential versus time graph at a static current density). Through CV, generally, 500 to 1000 continuous CV cycles are run, and after that, the shift in the overpotential at a particular current density is measured by comparing the linear sweep voltammetry (LSV) before and after these continuous cycles. From the other two methods, stability is evaluated by running the experiment for a long time either at a fixed potential or current density.

1.7 Scope of the work and objective of the thesis

For the fossil fuel-free future of the world, renewable energy technologies have become obligatory. Water splitting, rechargeable metal-air batteries and fuel cells are required to

produce and store renewable energy as well as for transformation into other forms of energy. In these devices, OER plays a critical role in producing pure oxygen; however, the sluggish kinetics of OER hinders the application of these devices at large-scale. In the water-splitting, in comparison to HER, OER is a more complex reaction. It entails a large overpotential to acquire the same current density, which presents a high kinetic barrier for OER. Besides the noble metal oxides IrO_2 and RuO_2, known as benchmarking OER catalysts, a profusion of materials has been used for OER, but still, a wide space is unexplored. Spinel materials, which are bimetallic and trimetallic oxides and metal-organic framework, a class of porous crystalline material, are recently gaining much attention towards OER. Their facile synthesis procedure opens a new scope to find substitutes for costly electrocatalysts for OER.

Considering these facts and cutting-edge applications of OER in renewable energy, this thesis is focused on the following objectives as given below:

- Synthesis of spinel oxides based electrocatalysts for OER studies. Nickel ferrite and cobalt-doped nickel ferrite (cobalt ferrite and cobalt nickel ferrite) are synthesised by a facile sol-gel method and employed for application.
- Synthesis of Co-MOF flower by a precipitation approach using cobalt salt and Anthranilic acid. Further, used as an active material to modify the glassy carbon electrode (GCE) for enhanced OER performance.
- Synthesis of spherical ZnDTO MOF by the complexation of Zinc salt and dithioxamide (DTO) ligand and preparing N/S/Zn–doped porous carbon matrix (NSC) by carbonizing them at different temperatures. Further, to examine the role of Zn on the catalytic performance of the materials, the thermally optimised carbon matrix is treated with a suitable acid and then the formation of Nanocomposites with Co_3O_4 to enhance the OER performance of these carbon matrix.

- Facile synthesis of Ni-Fe Prussian blue analogue nanocubes and their conversion into Nanocages and mixed oxide through control chemical etching and annealing in air, respectively for OER application.